

The Radio and Gamma Ray Connection of EGRET Blazars: Correlation, Regression, & Monte Carlo Analysis

S. D. Bloom ¹

Department of Physics & Astronomy, Hampden-Sydney College

Box 821, Hampden-Sydney, Virginia 23943

ABSTRACT

A comprehensive statistical analysis of the broadband properties of EGRET blazars is presented. This analysis includes sources identified as blazars in the Sowards-Emmerd publications. Using this sample of 122 sources, we find that there is a relationship $L_\gamma \propto L_r^{0.77 \pm 0.03}$ as well as a correlation between α_{og} and α_{ro} , and a correlation between radio luminosity and α_{og} . Through the use of Monte Carlo simulations, we can replicate the observed luminosity relationship if a synchrotron self-Compton model is assumed. However, this relationship can not be replicated if an external Compton scattering model is assumed. These differences are primarily due to beaming effects.

In addition it has been determined that the intrinsic radio luminosity of the parent sample falls in the range $10^{21} < L < 10^{30} \text{ Watts Hz}^{-1}$ and that the bulk Lorentz factors of the source are in the range $1 < \Gamma < 30$, in a agreement with VLBI observations.

Finally, we discuss implications for GLAST, successfully launched in June 2008.

Subject headings: gamma rays: observations

1. Introduction

During the lifetime of the Energetic Gamma-Ray Experiment Telescope (EGRET) instrument on board *Compton Gamma-Ray Observatory* (CGRO) 271 sources were detected with 66 being confidently identified as blazars in the Third EGRET Catalog (Hartman *et al.*

¹Visiting Scientist, National Radio Astronomy Observatory, Charlottesville, VA

1999). Many differing statistical analyses of these gamma ray detected blazars have been conducted, among them Fossati *et al.* (1998); Mucke *et al.* (1997). Some of these analyses concentrated on the direct statistical relationship between luminosities in the gamma-ray band and radio bands (Salamon & Stecker 1996; Stecker, Salamon, & Malkan 1993; Fan *et al.* 1998). Of these, most have used single dish radio data, but some have used VLBI fluxes (Zhou *et al.* 1997; Mattox *et al.* 1997), all at various radio frequencies > 1 GHz. In addition, Mucke *et al.* (1997) and Impey (1996) use Monte Carlo simulations to aid in interpreting these relationships. Though significant correlations are reported in all of these works, Mucke *et al.* (1997) show that in some cases these will result from a combination of variability and selection effects. To investigate the variability effects further, Zhang, Cheng, & Fan (2001) have compared their statistical results using time averaged data for the entire sample to similar results for a restricted sample for which data were available during high and low states. They report a similar significant correlation in each case and show that using time averaged data tends to under estimate the underlying linear regression slope (as applied to the logarithmic data).

Various models have been invoked to explain the origin of the gamma-ray emission of blazars and specifically, the radio gamma-ray correlation. Among these are the synchrotron self Compton (SSC) model (Bloom & Marscher 1996; Ghisellini, Maraschi, & Treves 1985) and various models in which the source of seed photons for scattering is from a source external to the jet (henceforth called ECS models for “external Compton scattering”). Dermer & Schlickeiser (1993) use the accretion disk as the source of soft photons whereas others (Ghisellini & Madau 1996) use broad-line region clouds as the source of soft photons.

Since the end of the EGRET mission there have also been several reanalyses of the significance of identifications of EGRET sources, particularly those of Mattox *et al.* (1997); Mattox, Hartman & Reimer (2001) and Sowards-Emmerd, Romani, & Michelson (2003, 2004). The Sowards-Emmerd, Romani, & Michelson (2003, 2004) survey excludes sources with $|b| < 10^\circ$ (the Mattox papers exclude sources with $|b| < 3^\circ$), and thus may exclude additional sources that are thought to be blazars (Sguera *et al.* 2004). Likewise, some work continues on identifying other individual sources, such as 3EG J0416+3650, possibly identified with 3C 111 (Sguera *et al.* 2006). In the eight years since the end of the CGRO mission, there has been substantial modification to the identifications given in the last catalog published by the EGRET team (Hartman *et al.* 1999), so we present a comprehensive statistical analysis including all potential identifications, using homogeneous criteria for inclusion in the sample (§2). We have also included various statistical techniques of survival analysis for the inclusion of upper and lower limits in the data (§3). We later discuss whether or not the results of the analyses are dependent on the precise source list. The approach used in understanding the physical implications of our results is to use a Monte Carlo technique (Lister & Marscher

1997) to generate multiple simulated samples under differing assumptions of overall theoretical or phenomenological model (§4,5), distribution of physical parameters such as bulk Lorentz factor (e.g., Gaussian, power-law, etc.) and selection effects. Additional physical implications of observed correlations and implications for the Gamma Ray Large Area Space Telescope (GLAST), successfully launched in June 2008, are discussed in §6,7.

2. Data

To construct a comprehensive list of identified gamma-ray blazars we have started with the Third EGRET Catalog (Hartman *et al.* 1999). We note that we are not re-evaluating the detections themselves. To add or remove sources from this list of identifications using uniform criteria, we have further used the guidance of Sowards-Emmerd, Romani, & Michelson (2003, 2004). Though other standards for inclusion or rejection do exist, we have used these particular surveys to keep inclusion criterion standard. We have taken the best blazar identifications with Figure of Merit (FoM) criterion greater than 0.25 (Sowards-Emmerd, Romani, & Michelson 2003, 2004). The FoM used here is a statistic that incorporates both radio and X-ray spectral information in evaluating the probability that a particular radio source is a match to the gamma-ray source. For sources with multiple possible identifications, we include the identification with the highest FoM value. Though the 0.25 cutoff is perhaps arbitrary, it is clear that well below this limit (at about 0.1), the probability for chance associations greatly increases (Sowards-Emmerd, Romani, & Michelson 2003). These authors and their current working group have not yet published an analysis for the sources between -40 and -90 declination. For these sources, we included all of the original catalog identifications, with the caveat that the more marginal identifications (i.e. counterparts with 8.4 GHz radio flux density < 0.5 Jy) could possibly not hold up to the analysis using the FoM criterion. The total number of such sources in this declination range is ten, with two below 0.5 Jy (the remainder all have flux density greater than 1 Jy at 8.4 GHz). We also note that we could be excluding candidate identifications heretofore unmentioned in this declination range. A summary of the available data used in our statistical analysis has been compiled in Table 1. Column(1) indicates the EGRET source name, column (2) indicates the best radio identification, followed by the redshift in column(3). Columns (4)-(6) give the monochromatic radio, optical and gamma ray luminosities, respectively (all have units of $\text{joules sec}^{-1} \text{ Hz}^{-1}$). If the redshift is unknown, we substitute with $z=1$. There are no significant changes in the results if we use other assumptions, such as $z=0.5$. To calculate the radio luminosity we use the 8.4 GHz flux densities and spectral indices (Column (7)) between 1.4 and 8.4 GHz of Sowards-Emmerd, Romani, & Michelson (2003, 2004) except for the lowest declination sources discussed above. For these, we extract the similar radio data from the NASA

Extragalactic Database (NED) to calculate the spectral index between 1.4 and 8.4 GHz. Henceforth we use $F_\nu \propto \nu^{-\alpha}$ for defining spectral indices. In calculating the optical luminosities we use recent V magnitudes extracted from NED (when available), and we derive an optical flux density and monochromatic luminosity from this magnitude using the conversions of Bessel (1979). Sowards-Emmerd, Romani, & Michelson (2003, 2004) also provide archival R and B magnitudes from the USNO catalog (Monet *et al.* 2003), which we have used to interpolate a V value if we did not otherwise have a reference for a V magnitude. In a few cases we only had O magnitudes from the POSS-I survey or 2MASS infrared magnitudes, and thus need to extrapolate to the V band. For sources that have no optical or near infrared magnitudes in the literature, and that were not detected in the POSS-I, SERC-J, or POSS-II we assume magnitude upper limits equal to the appropriate plate limits of the survey (eg., O=21.5, E=20 for POSS-I McMahon *et al.* (2002)) and derive upper limits to the optical luminosities accordingly. The gamma-ray luminosities are determined from the flux and spectral index (Column (8)) given in Hartman *et al.* (1999). We use the formula of Thompson *et al.* (1996) to derive an exact 400 MeV flux. If the spectral index is not known, we assume it is 1.0 (note that we are referring to the energy spectral index and not the photon index). In all cases we use the co-added flux over all viewing periods. In the absence of simultaneous data at all wavelengths, this is a better representation of broad band properties than any single value. Each of the luminosities is calculated using equation (2) of Lister & Marscher (1997) and assumes a flat Λ cosmology with $\Omega_m = 0.3$ and $\Omega_\Lambda = 0.7$ (Perlmutter *et al.* 1997). Though the luminosity distance can be calculated via numerical integration, it is preferred to find an analytic expression, especially for use in the Monte Carlo simulations where such a calculation will have to be performed many millions of times. Pen (1999) offers such an option; however this formula can differ from the numerically determined value by over 5%. Therefore, a polynomial fit to the numerical solutions is determined for the redshift range $z=0-5$ using the Wolfram Research program *Mathematica* to attain a more accurate approximation. When luminosity distances determined via this polynomial fit were compared with the results of a direct numerical integration, the agreement was well within 1% for the range $0.1 < z < 4.0$; however, at redshifts outside of this range, the disagreement is as large as 7%. Column(9) shows the broadband spectral index, α_{ro} gives the index α_{og} . Column (11) has the gamma-ray variability parameter, δ_{var} , as determined by Nolan *et al.* (2003). Column (12) gives the references for the data, where the first reference is for redshift, the second for the radio data, the third for the optical magnitudes, and the fourth for the gamma ray data.

3. Statistical Analysis

We have evaluated the strength and significance of correlation between monochromatic luminosities using non-parametric methods, such as Kendall’s τ (Kendall & Gibbons 1990). These results are given in Table 2. Column(1) gives the independent variable, Column(2) the dependent variable, Column(3) the number in the sample, Column(4) Kendall’s τ statistic, Column(5) the probability of the null result for this statistic, Column(6) the Spearman’s ρ statistic, Column(7) the probability of the null result for this statistic, and in Column(8) the regression technique used. Here BJ refers to the Buckley-James method, EM refers to the EM method and SB refers to Schmitt’s binned regression, as explained in the references that follow. Column(9) gives the linear regression slope, and Column(10) the linear regression Y-intercept. In some cases, we have upper and lower limits to measured values, and to take this into account, we use the proper correlation and regression techniques as discussed in Feigelson & Nelson (1985); Isobe, Feigelson & Nelson (1986) and utilized in the ASURV software package. In reporting correlation coefficients, probabilities and regression fits we adopt the format of Mucke *et al.* (1997). That is, we report three significant digits down to 0.100. Between 0.010 and 0.100 we report two significant digits, and for all numbers with values below 0.01, we only report with 1 significant digit.

Most notably, we determine that there is a strong correlation between gamma ray and radio luminosity (Figure 1 and Table 2). In order to determine whether the correlation is affected by including the sources with FoM < 1 (the lower confidence identifications), we recalculate the correlation and regression coefficients while retaining only the 76 sources with FoM > 1 . The strength of the correlation is similar, with a very slight steepening of the regression slope (0.78 instead of 0.77, which is within the range of the uncertainty of the correlation slopes). If the sources with declination below -40° are also excluded, the correlation slope flattens slightly to 0.73. In all though, correlation is not significantly altered by such changes to the source list.

For some correlations, we must account for the effect of a third variable, using partial correlation analysis (Padovani 1992). Results of our partial correlation analysis are given in Table 3. Column(1) gives the independent variable, Column(2) the dependent variable, Column(3) the third variable, Column(4) the number in sample, Column(5) Kendall’s τ , and Column(6), the probability of the null result. Examples of this are the need to take into account the correlation of all luminosities on redshift, and the dependence of several broad band spectral indices on optical luminosity. In particular we note that the strong correlation between gamma ray and radio luminosity is significantly weaker, though still significant, once we account for the partial correlation with redshift. Similarly, the correlation between the α_{ro} and $\alpha_{o\gamma}$ still persists, even after the effect of the common dependence on optical

luminosity is negated. We use the Kendall’s τ coefficient for this purpose, since to date it is the only coefficient for which there are methods to take into account censored data (Akritas & Siebert 1996). A detailed discussion of the physical models for the luminosity correlation is addressed in §4, §5. Further discussion of the remaining correlations is deferred to §6.

4. Physical Models

Our approach in this section is to see if particular models can be used to explain our statistical results above, particularly the radio and gamma-ray luminosity relationship. A radio and gamma-ray luminosity correlation would naturally be expected given any of the non-thermal inverse Compton models linking low energy emission with gamma rays, such as in Bloom & Marscher (1996). As noted above, this luminosity correlation holds even after we take the effect of redshift into account. A linear or nearly linear correlation is possible within the synchrotron self-Compton (SSC) model if the range of possible physical parameters, particularly the optically thin spectral index, Thomson optical depth and electron energy cutoffs do not vary too greatly in the sample. This can be illustrated by following Marscher (1987) for a spherical homogeneous source:

$$\frac{L_{\nu c}}{L_{\nu s}} = c_3(\alpha) N_0 R \ln\left(\frac{\nu_m}{\nu_2}\right) \left(\frac{\nu_c}{\nu_s}\right)^\alpha \quad (1)$$

Where $L_{\nu c}$ is the frequency dependent Compton luminosity, $L_{\nu s}$ is the frequency dependent synchrotron luminosity. c_3 is a function of spectral index, tabulated in Marscher (1987), N_0 is the normalization factor of the energy dependent electron density distribution, and R is the radius of a spherical source. ν_m refers to the spectral turnover frequency in a plot of flux density versus frequency, and ν_2 is the upper frequency cutoff in a similar plot. A correction to this formula needs to be applied if the observed gamma-rays are at a frequency beyond the high end spectral cutoff for Compton scattering, or if the synchrotron photons are observed at a frequency at which the source is believed to be optically thick or partially opaque. The logarithmic term only varies a small amount for large changes in the parameters, so this term can usually be neglected relative to the others. The function of α can vary over several orders of magnitude, but can be roughly constant if the optically thin spectral index of the sample is narrowly distributed. The factor of $N_0 R$, proportional to the Thomson optical depth, would also have to be tightly constrained. Using a somewhat different formulation, Ghisellini *et al.* (1998) calculate a particle injection compactness parameter, which is also proportional to the Thompson optical depth. They show that this parameter,

though distributed over 4 orders of magnitude for a sample of 51 EGRET blazars, has a clear peak value (over half of the blazars with a value within 1 order of magnitude of the peak). Thus, in adopting a linear model for use in the following Monte Carlo analysis, this parameter can be drawn randomly from a sharply peaked distribution. It is not as evident that these arguments can be extended to a relationship such as that observed, $L_\gamma \propto L_r^{0.77}$. We explore this possibility below.

Alternatively, the gamma-ray luminosity can be produced by an external Compton scattering process (ECS)(Dermer & Schlickeiser 1993; Lister 1999). In this particular model the source of the soft photons is the accretion disk, and these photons scatter off of a plasma of relativistic electrons in a blob. Adapting the formulas of Dermer, Schlickeiser, & Mastichiadis (1992) to our notation:

$$\frac{L_{\nu c}}{L_{\nu, acc}} = \frac{R^3}{6r^2} \sigma_T (m_e c^2)^{-2\alpha} N_0 \delta^{2\alpha+4} (\nu/\nu_o)^{-\alpha}$$

Here, the luminosity ratio is between the observed Compton luminosity in the gamma-ray range and the observed accretion luminosity. R refers to the radius of the blob, assuming it is spherical, and r refers to the distance between the blob and the accretion disk. σ_T refers to the Thomson scattering cross-section, $m_e c^2$ refers to the electron rest mass, N_0 has the same meaning as above. δ is the Doppler factor to correct for bulk relativistic motion of the emitting plasma and is defined by:

$$\delta \equiv \frac{1}{\Gamma(1 - \beta \cos \theta)} \quad (3)$$

Here β has the usual meaning of ratio of bulk speed to that of light in a vacuum, and θ is the angle between direction of the bulk flow and the line of sight of the observer. The power to which the Doppler factor is raised is dependent on the structure of the emitting region (discrete blobs vs. continuous jet). The formula above is correct for discretely emitting blobs. For a continuous jet, the power is reduced by one (Dermer 1995). It has been suggested that the synchrotron luminosity can be proportional to the ultraviolet luminosity of the seed photons (Ghisellini & Madau 1996), thus providing a direct relationship (though not necessarily linear) between the gamma-ray and radio luminosity within the framework of the ECS model. Furthermore, the underlying radio and gamma-ray correlation may also be explained by other means, since the gamma-ray luminosity in all relativistic Compton scattering models is proportional to the Thomson optical depth and the intrinsic radio luminosity can be proportional to the Compton optical depth via the parameter N_0 and R . Other source parameters, such as the magnetic field, would have to fall into a narrow range for the sample in order for this correlation to hold.

5. Monte Carlo Simulations

The goal of our Monte Carlo simulations is to generate the luminosities and flux densities of a hypothetical sample that, in principle, mimics the sample of gamma-ray detected blazars discussed above. To do that we need to define a radio luminosity function from which we will randomly draw to create the sample. We will also need a distribution of Lorentz factors which will be used in determining Doppler beaming factors needed to transform between observer frame luminosities and intrinsic luminosities. In addition, we will need a model that determines what the gamma-ray luminosity will be for a given radio luminosity. We will limit ourselves to the models discussed above. Lastly, we will need to adopt a cosmological model in order to determine redshifts corresponding to randomly chosen enclosed volumes of space. We can then determine both radio and gamma-ray flux densities using these redshifts and the adopted cosmological model. Following Lister & Marscher (1997) we have used an assumed radio luminosity function of the form:

$$\rho(L) \propto L^{-g} \quad (4)$$

valid between L_1 and L_2 . We have adopted a luminosity evolution function:

$$L(z) = L(z=0) \exp[T(z)/\tau] \quad (5)$$

Where $T(z)$ is the look-back time and τ is a constant in the approximate range of 0.1-0.5 that determines the degree of evolution.

We have also assumed a distribution of Lorentz factors for which:

$$N(\Gamma) \propto \Gamma^{-s} \quad (6)$$

valid between Γ_1 and Γ_2 and a linear model connecting gamma-ray and radio luminosities, i.e., the inverse Compton models discussed above, to generate a simulated sample with Monte Carlo techniques and then use the corresponding distributions (luminosity, redshift, flux density, etc.) and correlation diagrams to assess the validity of the model. We express these models using the following equations :

$$L_{\gamma,o,ssc} = K_{ssc} L_{r,i} \delta^{3+\alpha} \quad (7)$$

$$L_{\gamma,o,ecs} = K_{ecs} f(\beta, \theta) L_{r,i} \delta^{4+2\alpha} \quad (8)$$

Here, $L_{\gamma,o,ssc}$ and $L_{\gamma,o,ecs}$ refer to the predicted gamma-ray luminosities in the observer’s frame, using the SSC and ECS models respectively. The K constants depend on the parameters discussed above, $L_{r,i}$ refers to the intrinsic radio luminosity, and the remaining factors are the appropriate functions of Doppler factors for SSC or ECS assuming that the radiation is from discrete blobs (Lister 1999). As mentioned above, the powers in each case are reduced by one for the case of a continuous jet.

Lister & Marscher (1997) rigorously determines radio luminosity function parameters based on simulations of the Caltech-Jodrell Bank sample (CJ-F, as labeled by Lister & Marscher (1997)), taking into account distributions of bulk Lorentz factors, redshifts, and luminosities. Cara & Lister (2007) have recently arrived at comparable results for the similar MOJAVE sample (though the luminosity and redshift ranges differ somewhat). We begin by adopting the parameters that Lister & Marscher (1997) derived for the CJ-F sample. We expect the CJ-F parent population to be very similar to that of our sample, because it is selected for flat spectrum, compact structure and 5 GHz total flux density > 0.35 Jy. Additionally we take into account beaming effects appropriate for the SSC or ECS model. Then, assuming both SSC and ECS in turn, the gamma-ray luminosity and flux density is determined for each source. In generating the gamma-ray luminosities from the intrinsic radio luminosities we assume a power-law distribution of the K values discussed above in Equations 7 and 8. This is an arbitrary choice of distribution, but the precise values of power-law slope and cutoffs do not significantly effect the results. We then generate 122 sources with gamma-ray flux that could have been detected by EGRET. We adjust the gamma-ray flux density limit to be slightly lower than that of EGRET (about 85 %) to allow for a proportion of upper limits that is similar to that we see in our observed sample. In looking for agreement between the simulated population and the observed one, we use the two distribution Kolmogorov-Smirnov test on the distributions of luminosity, redshift and flux density. The D_{KS} statistic is then used to measure the discrepancy between the two distributions. D_{KS} is defined as (Press *et al.* 1986):

$$D_{KS} \equiv \max|S_{N1}(x) - S_{N2}(x)| \quad (9)$$

That is, D_{KS} is the maximum difference (absolute value) between the two distribution functions, $S_{N1}(x)$ and $S_{N2}(x)$. The distribution function is defined to be the probability that the particular value of the parameter in question is less than x. A value of D_{KS} near zero indicates agreement between the distribution functions, whereas a value near 1 indicates a large discrepancy. The associated probability is also determined following Press *et al.* (1986). In this case, a probability approaching 1 indicates a high probability for agreement between the distributions. For distributions that include upper limits we use the corresponding tests

using the ASURV program (this is only an issue for the gamma ray flux densities and luminosities). Among these tests are the Gehan generalized Wilcoxon test and the Peto & Peto Generalized Wilcoxon test. The results of these tests are discussed below. We have applied these methods using the parameters of Lister & Marscher (1997), summarized in Table 4. In Table 4, Column (2) gives L_1 , Column(3) gives L_2 and they refer to the lower and upper luminosity limits of the intrinsic luminosity function. Column (4) gives g and refers to the luminosity function power law slope. Column(5) gives Γ_1 , Column(6) gives Γ_2 and Column(7) gives s . These labels refer to the lower bulk Lorentz factor distribution limit, upper bulk Lorentz factor distribution limit and the slope of the power law, respectively. Column (8) gives τ and in this case refers to the evolution parameter, assuming an exponential evolution model (see Equation 5). Column(9) gives z_{min} and is the lower limit to the redshift distribution and Column(10) gives z_{max} and is the upper limit. Column (11) gives h as discussed in §2, Column (12) gives the minimum value of K , Column (13) the maximum value of K and Column (14) gives the slope of the power-law distribution of K , where K refers to either K_{ssc} or K_{ecs} (Equations 7 and 8), whichever is appropriate for the simulation indicated. Applying the values assumed by Lister & Marscher (1997) does not immediately lead to good agreement between the observed and modeled distributions (see Table 5). For models marked "Lister SSC" we have adopted an SSC model to generate simulated gamma ray luminosities and for "Lister ECS" we have adopted an ECS model to generate simulated gamma ray luminosities. Next we have explored parameter space to determine where better models might lie. Since the number of parameters and the possible range of parameters is large, there are likely to be multiple models that would have similar agreement as seen by a K-S test. The results that give the lowest value of D_{KS} (Equation 9) with high significance are summarized in Table 5 for the SSC and ECS models. Column(2) gives the D_{KS} value for the radio luminosity function and Column(3) gives the associated probability that the distributions are drawn from the same parent population. Column(4) and Column(5) give the same results for the gamma ray luminosity distributions, whereas Columns (6) and (7) do so for redshift, and Columns(8)-(11) do so for the radio and gamma-ray flux density distributions, respectively. These results can also be visually inspected in Figures 2-11. There is only weak agreement between the observed and predicted distributions for either SSC or ECS. For the special case of the gamma-ray flux and luminosity distributions (which have limits as well as measured values), we have used the tests discussed above, and generally the associated probabilities (for agreement of the two distributions) for these tests fall in the range of 0.0002-0.0015 for SSC and 0.0001-0.0010 for ECS, thus also only very weakly confirming the SSC or ECS hypothesis. The parent population in these simulations was approximately 30 million for SSC and 300 million for ECS. Both models require a range of Lorentz factors of about 1-30. This is the approximate range inferred by VLBI observations (Cohen *et al.* 2007). However, some authors have made the argument that these bulk Lorentz

factors may not pertain to the same portion of the jet from which the gamma ray emission originates (Georganopoulos & Kazanas 2003).

A closer look at Figures 2-11 show some features that are not as evident from just comparing results of Kolgomorov-Smirnov tests. A comparison of the radio luminosity distributions (Figures 2a,2b,& 7) shows that assuming an SSC or ECS model lead to similar results. Both the SSC and ECS distributions have peak values near 10^{27} Watts Hz⁻¹, with approximately 24 % of the sample having values near the peak for SSC and 21 % for ECS. The observed distribution of radio luminosity peaks near 10^{28} Watts Hz⁻¹ with approximately 33 % of the sample in the bin nearest to the peak. However, in conjunction with the redshift and flux density distributions we do see some important differences between the predictions of the SSC and ECS model, and can pin point particular observations that will be necessary in the GLAST era for differentiating these models using the methods we have discussed above. For instance, when looking at the simulated distributions of radio flux density (Fig. 4a, Fig. 9), the simulated distribution assuming the SSC model is clearly peaked close to about 0.3 Jy, whereas the same distribution for ECS is peaked close to 1.5 Jy. The observed distribution is peaked closer to 0.3 Jy and is more similar in overall shape to the predicted SSC distribution (Fig. 4b). Ongoing radio monitoring of GLAST detected sources (or at least updated to these older survey flux densities) will be critical for determining the true observed distribution to be used for comparison to models. In addition, we can see that the redshift distribution (Fig. 6a) with SSC assumed is nearly identical to the corresponding distribution with ECS assumed (Fig. 11). Though the observed redshift distribution (Fig. 6b) is also peaked near $z=1$, this is at least in part due to the assumed redshifts of $z=1$ for 13% of the sample. An additional challenge in the GLAST era will be obtaining redshifts for entire large samples (possibly thousands of new quasars that have not yet been optically identified or observed spectroscopically). It is a bit harder to discern significant differences between the ECS and SSC predictions for either gamma-ray luminosity or gamma-ray flux density. However, a significant increase in sensitivity for GLAST should clarify the nature of the low-end of each of these diagrams. For example, we now can only see a very large drop-off in all of the flux densities near 10^{-11} Jy. This is caused by the flux detection limit of EGRET. In addition, the dramatic increase in number of gamma-ray detected sources to thousands (Padovani 2007) will clarify the shape of these distributions and increase the conclusiveness of comparisons to theoretical predictions.

We have also used the Monte Carlo results to generate simulated luminosity-luminosity correlation plots between $\log L_\gamma$ and $\log L_r$ by assuming, in turn, the SSC and ECS models. The SSC simulations generate the relationship $L_\gamma \propto L_r^{0.74 \pm 0.02}$, in agreement with observations. However, assuming the ECS model generates results with $L_\gamma \propto L_r^{0.95 \pm 0.02}$ (the results are plotted in Figures 12a and 12b). This clearly shows that though the assumed underlying

physical models in both the SSC and ECS case are linear between L_γ and L_r , selection effects can lead to a simulated sample that shows a non-linear relationship between the luminosities. This effect is more pronounced for the SSC case. This is potentially an effect caused by Doppler beaming factors raised to different exponents (dependent on spectral shape). For instance, in the SSC case, if the exponents for the beaming factors are identical for both the radio and gamma ray part of the spectrum, then we would expect no change in going from the intrinsic luminosity correlations and the observed ones. However, in our model we do account for the possibility that the gamma-ray spectrum is considerably steeper than the radio spectrum. This leads to somewhat different exponents for the Doppler beaming factors that are going into an overall beaming correction that is applied to the intrinsic radio and gamma ray luminosities. There are two additional effects which we have not modeled, but may contribute to the observed luminosity correlation. In particular, the radio source and gamma-ray source may not be spatially coincident, and may thus have different bulk Lorentz factors, as discussed above. Also, the bulk Lorentz factors may be dependent on radio luminosity (Lister & Marscher 1997).

Though similar effects are also at work with ECS process, it is less pronounced in our case due to a selection effect. That is, because the range of K_{ecs} is very narrow, and also has relatively low values, only the sources with the highest values of Lorentz factors are detected in gamma rays. Thus, relative to the SSC case, the Doppler factors are closer to being constant for the sample. Overall, this leads to a relationship between the gamma-ray and radio luminosities that is closer to being linear.

6. Additional Correlations

In addition to the luminosity correlation that we have discussed at length we have also observed other significant correlations for the sample. The origin of the broad band spectral index correlation, α_{og} vs. α_{ro} (Table 2), becomes clear if we consider the conclusions of Fossati *et al.* (1998). They show that gamma-ray dominance (the ratio of gamma-ray luminosity to luminosity at the model dependent synchrotron peak of the SED) is positively correlated with the maximum frequency of the lower energy peak of the SED. In a simple homogeneous source, this lower energy peak corresponds to the upper synchrotron cutoff frequency discussed above. Ghisellini *et al.* (1998) show that this correlation is a proxy for the underlying physical relationship between the maximum relativistic electron energy (on which the low frequency peak strongly depends) and the ratio of the Compton and synchrotron luminosities. For a model in which both an internal (SSC) and external (ECS) radiation field are present, an increase in the energy density of the external field leads to

an increase in Compton cooling and thus a decrease in the maximum electron energy and an increase in the Compton gamma-ray luminosity (Ghisellini *et al.* 1998). Fossati *et al.* (1998) further show that observed optical flux density can be substituted for the (model dependent) synchrotron peak flux density without loss of the Compton dominance/spectral peak frequency correlation. We utilize this useful substitution below. Fossati *et al.* (1998) also show that both α_{rx} and α_{ro} are separately but similarly correlated with this same spectral maximum frequency, so that the latter may be substituted for the former in the absence of X-ray data. Though we have limited spectral data for many sources, and thus can't confirm this related correlation for our own sample, the same reasoning should apply to our sample, and thus we make this substitution as well. Thus the correlation of α_{og} and α_{ro} is a possible indicator of the relationship between dominance of gamma-rays produced by the ECS process and maximum electron energy. However, it is also possible that the broad band spectral index correlation is not independent of the radio/gamma-ray luminosity correlation discussed above. This is especially true if we take into account the common dependence of both spectral indices on optical luminosity (Table 3). Recent surveys have also suggested that the aforementioned correlations discussed in Fossati *et al.* (1998) and Ghisellini *et al.* (1998) may be due in part to selection effects (Anton & Browne 2005; Nieppola, Tornikoski, & Valtaoja 2006). For instance, the low luminosity objects of Fossati *et al.* (1998) were mainly X-ray selected, favoring selection of objects with SEDs peaked at higher frequencies, whereas the high luminosity objects were mainly radio selected, thus favoring the selection of objects with SEDs peaked at lower frequencies (Anton & Browne 2005).

The correlation between radio luminosity and gamma-ray dominance (which in our analysis would be characterized by α_{og}), originally seen by Fossati *et al.* (1998) is also seen here, after more than doubling the sample size. Here, because of the way the broad band indices are defined, a lower value of α_{og} corresponds to greater gamma-ray dominance. This correlation is further evidence for a blazar sequence defined by relative importance of the ECS model at higher luminosities.

We have also examined a possible correlation between all parameters individually and the gamma-ray variability (Nolan *et al.* 2003) and find only a weak anti-correlation between gamma-ray spectral index, α_γ , and variability (as parameterized by Nolan *et al.* (2003); see Table 1). This may be related to a spectral hysteresis effect observed by Nandikotkur *et al.* (2007) for a sample of 26 particularly bright and well observed blazars. These authors find that during gamma ray flares the spectral index first tends to flatten with increasing flux, and then returns to a steeper index as the flare ends. Thus, it is plausible that if a blazar is more highly variable there will be an increasing chance of observing it while its spectral index is flatter than for other blazars that are not gamma ray variables.

7. Conclusions and Implications for GLAST

After taking into account statistical tests and Monte Carlo analysis, we find the following:

1. For this sample of 122 gamma-ray blazars there is a strong correlation between radio and gamma ray luminosity which persists even after the effects of redshift and limits are taken into account. The correlation is of the form $L_\gamma \propto L_r^{0.77}$. This correlation remains with similar regression coefficients even when only the strongest 76 candidates are included in the sample.
2. There is a correlation between α_{og} and α_{ro} as well as a correlation between L_r and α_{og} . Each correlation is consistent with the increasing dominance of the SED by gamma ray luminosity as the maximum relativistic electron energy decreases and the increasing importance of the ECS process at high radio luminosities and low maximum electron energy.
3. A detailed simulation of source statistics using Monte Carlo techniques shows that the relationship $L_\gamma \propto L_r^{0.77}$ can only be reproduced assuming the SSC model. Though the assumed intrinsic physical model in the source frame is of the form $L_\gamma \propto L_r$, selection effects lead to a simulated sample with the relationship described above. This effect is much less significant when ECS is assumed as the underlying model. However, upon also comparing the observed and simulated distributions of the luminosities, flux densities and redshifts, both the SSC and ECS models are only weakly consistent with the data, assuming linear dependence of intrinsic gamma ray luminosity on intrinsic radio luminosity. Taken together with the previous results, this would suggest that if either SSC or ECS is indeed responsible for the gamma ray emission, a more complex model is likely needed. In addition, effects of evolution and assumed cosmologies can be explored in more detail.

In the GLAST era, our findings can be clarified in the following ways. Acquiring more gamma-ray data, including, particularly, detections of new dim sources near the GLAST detection limit will clarify whether the correlations we find are caused by truncation effects due to the flux limits of our instruments, or whether this is due, at least in part, to physical causes, at least down to the new limit established by GLAST.

In order to predict what we might see with GLAST, we can extend our observed radio/gamma ray luminosity correlation down to lower luminosities than what are covered in Figure 1. A radio luminosity of $1.25 \times 10^{24} \text{ Watts Hz}^{-1}$ would lead to a gamma ray luminosity of approximately $4.98 \times 10^{13} \text{ Watts Hz}^{-1}$. We can then covert these luminosities

to flux densities for a range of potential redshifts. For $z=0.1-1.1$ the radio flux density would be in the range of 0.8-60 mJy and the gamma-ray flux density would be in the range, 3.3×10^{-14} - 2.4×10^{-12} Jy. Greater values of redshift would lead to even lower flux density values. Most of the range of radio flux densities ($> \text{few mJy}$) would be detectable by the Green Bank Telescope (GBT), with the lower limit detectable with the Very Large Array (VLA)(Condon 2008). Assuming that the sensitivity of GLAST is approximately 2.8×10^{-13} Jy at 100 MeV, these sources would only be detected if $z < 0.2$. A radio luminosity of $1.58 \times 10^{23} \text{ Watts Hz}^{-1}$ corresponds to a gamma-ray luminosity of $1 \times 10^{13} \text{ Watts Hz}^{-1}$. The radio flux density would fall in the range of 0.1-8 mJy for $z=0.1-1.1$. These sources could potentially be radio detectable with the VLA under optimal conditions. At the higher flux density limit it would also be possible to detect with GBT, especially at higher frequencies (i.e., 40-50 GHz)(Minter 2008). However, if the regression slope were actually closer to 1, implying a direct proportionality between radio and gamma ray luminosities, then radio sources in the same luminosity, redshift and flux ranges discussed above would not be detected in gamma rays at all. In short, for the observed luminosity relationship for EGRET blazars to be appreciably extended down to lower luminosities with GLAST detections, then a large percentage of GLAST sources near the detection limit would have radio flux densities about 10 mJy or greater (and $z < 1$). Several authors have stated that the predicted number of blazars to be detected by GLAST roughly matches with the sky density of flat spectrum radio sources down to 50 mJy at 5 GHz (Padovani 2007) and 65 mJy at 8.4 GHz (Healey *et al.* 2007). However, our results show that a large number of GLAST sources would be detected at even lower radio flux densities if the luminosity relationship we observe for EGRET sources also holds up for GLAST sources. It is very likely that many new radio observations would be required in any of the cases mentioned above, but especially for cases in which the putative radio source may not even be in any previous catalog.

From a theoretical perspective, confirmation of the previously determined correlation between gamma-ray and radio luminosities will lead to confirmation of SSC, though the precise agreement would have to be re-analyzed with these new data.

The author thanks M. Lister for many useful discussions and the anonymous referee for abundant constructive comments. S. Bloom would like to acknowledge the generosity of the National Radio Astronomy Observatory (NRAO) during his stay as a Visiting Scientist at NRAO Headquarters in Charlottesville, VA. S. Bloom would also like to acknowledge several Summer Faculty Fellowship grants from Hampden-Sydney College.

This work has also made extensive use of the NASA Extragalactic Database (NED) and NASA's Astrophysics Data System Bibliographic Services (ADS).

REFERENCES

- Akritas, M. G. & Siebert, J. 1996, MNRAS, 278, 919
- Anton, S. & Browne, I. W. A 2005, MNRAS, 356, 225
- Bessel, M. 1979, PASP, 91, 589
- Bloom, S. D. & Marscher, A. P., ApJ, 461, 657
- Bloom *et al.* 2004, AJ, 128, 56
- Cara, M. & Lister, M. L. 2007, ApJ, in press
- Caroll, S. M. & Press, W. H. 1992, ARA&A, 30, 499
- Cohen, M. H., Lister, M. L., Homan, D. C., Kadler, M., Kellermann, K. I., Kovalev, Y. Y., Vermeulen, R. C. 2007, ApJ, 659, 232
- Condon, J. J. 2008, private communication
- Dermer, C. D., Schlickeiser, R., Mastichiadis, A. 1992, A&A, 256, L27
- Dermer, C. D. & Schlickeiser, R. 1993, ApJ, 416, 458
- Dermer, C. D. 1995, ApJ, 446, L63
- Fan, J. H., Adam, G., Xie, G. Z., Cao, S. L., Lin, R. G., Copin, Y. 1998, A&A, 338, 27
- Feigelson, E. D. & Nelson, P. I. 1985, ApJ, 293, 192
- Fossatti, G., Maraschi, L., Celotti, A., Comastri, A., Ghisellini, G. 1998, MNRAS, 299, 433
- Fouque, P., Durand, N., Bottinelli, L., Gougenheim, L., Patureli, G. 1992, *Catalogue of Optical Radial Velocities*
- Ghisellini, G., Maraschi, L., Treves, A. 1985, A&A, 146, 204
- Ghisellini, G. & Madau, P. 1996, MNRAS, 280, 67
- Ghisellini, G., Celotti, A., Fossati, G., Maraschi, L., Comastri, A. 1998, MNRAS, 301, 451
- Georganopoulos, M. & Kazanas, D. 2003, ApJ, 594, L27
- Halpern, J. P., Eracleous, M., Mattox, J. R. 2003, AJ, 125, 572
- Hartman, R. C. *et al.* 1999, ApJS, 123, 79

- Healey, S. E. *et al.* 2007, ApJS, 171, 611
- Hewitt, A. & Burbidge, G. 1987, ApJS, 63, 1
- Impey, C. 1996, AJ, 112, 2667
- Isobe, T., Feigelson, E. D., Nelson, P. I. 1986, ApJ, 306, 490
- Kendall, M. & Gibbons, J. D. 1990, *Rank Correlation Methods* (New York: Oxford University Press)
- Landt, H., Padovani, P., Perlman, E. S., Giommi, P., Bignall, H., Tziomis, A. 2001, MNRAS, 323, 757
- Lauberts, A. & Valentijn, G. A. 1989, *A Surface Photometry Catalog of ESO-Uppsala Galaxies*, European Space Observatory, Garching
- Lister, M. & Marscher, A. P. 1997, ApJ, 476, 572
- Lister, M. 1999, Ph. D. dissertation, Boston University
- Liang, E. W. & Liu, H. Y. 2003, MNRAS, 340, 632
- Marscher, A. P. 1987, in *Superluminal Radio Sources*, eds. J. A. Zensus & T. J. Pearson (Cambridge: Cambridge University Press), 280
- Mattox, J. R. *et al.* 1997, ApJ, 481, 95
- Mattox, J. R., Hartman, R. C., & Reimer, O. 2001, ApJ, 135, 155
- McMahon, R. G. White, R. L., Helfand, D. J., Becker, R. H. 2002, ApJS, 143, 1
- Minter, T. 2008, private communication
- Monet, D. G. *et al.* 2003, AJ, 125, 984 J., Mirabal, N., Gotthelf, E. V. 2002, ApJ, 574, 694
- Mucke, A. *et al.* 1997, A&A, 320, 33
- Nandikotkur, G. *et al.* 2007, ApJ, 657, 706
- Nieppola, E., Tornikoski, M., & Valtaoja, E. 2006, A&A, 445, 441
- Nolan, P. L., Tompkins, W. F., Grenier, I. A., Michelson, P. F. 2003, ApJ, 597, 615
- Padovani, P. 1992, A&A, 256, 399

- Padovani, P. 2007, *The First GLAST Symposium*, eds. S. Ritz, P. Michelson, C. Meegan, p. 19
- Perlmutter, S. *et al.* 1997, ApJ, 483, 565
- Pen, U. L. 1999, ApJS, 120, 49
- Press, W. H., Flannery, B. P., Teukolsky, S. A., & Vetterling, W. T. (Cambridge: Cambridge University Press), 472
- Salamon, M. H. & Stecker, F. W. 1996, ApJ, 430, 21
- Sguera, V., Malizia, A., Bassani, L., Stephen, J. B., Di Cocco 2004, A&A, 414, 839
- Sguera, V., Bassani, L., Malizia, A., Dean, A. J., Landi, R., Stephen, J. B. 2006, A&A, 430, 107
- Sowards-Emmerd, D., Romani, R. W., Michelson, P. F. 2003, ApJ, 590, 109
- Sowards-Emmerd, D. , Romani, R. W., Michelson, P. F. 2004, ApJ, 609, 564
- Stecker, F. W., Salamon, M. H., Malkan, M. A. 1993, ApJ, 410, 71
- Stoeck, J. T. *et al.* 1991, ApJS, 76, 813
- Thompson, D. J. *et al.* 1997, ApJS, 107, 227
- Torres, D. F., Pessah, M. E., & Romero, G. E. 2001, *Astron. Nachr.*, 4, 223
- Veron-Cetty, M. P. & Veron, P. 2001, A&A, 374, 92
- Wisotzki, L. *et al.* 2000, A&A, 358, 77
- Wright, A. & Otrupcek, R 1990, *Parkes Radio Catalogue*, Australian Telescope National Facility
- Zhang, L., Cheng, K. S., Fan, H. 2001, PASJ, 53, 207
- Zhou, Y. Y., Lu, Y. J., Wang, T. G., Yu, K. N., Young, E. C. M. 1997, ApJ, 484, 47

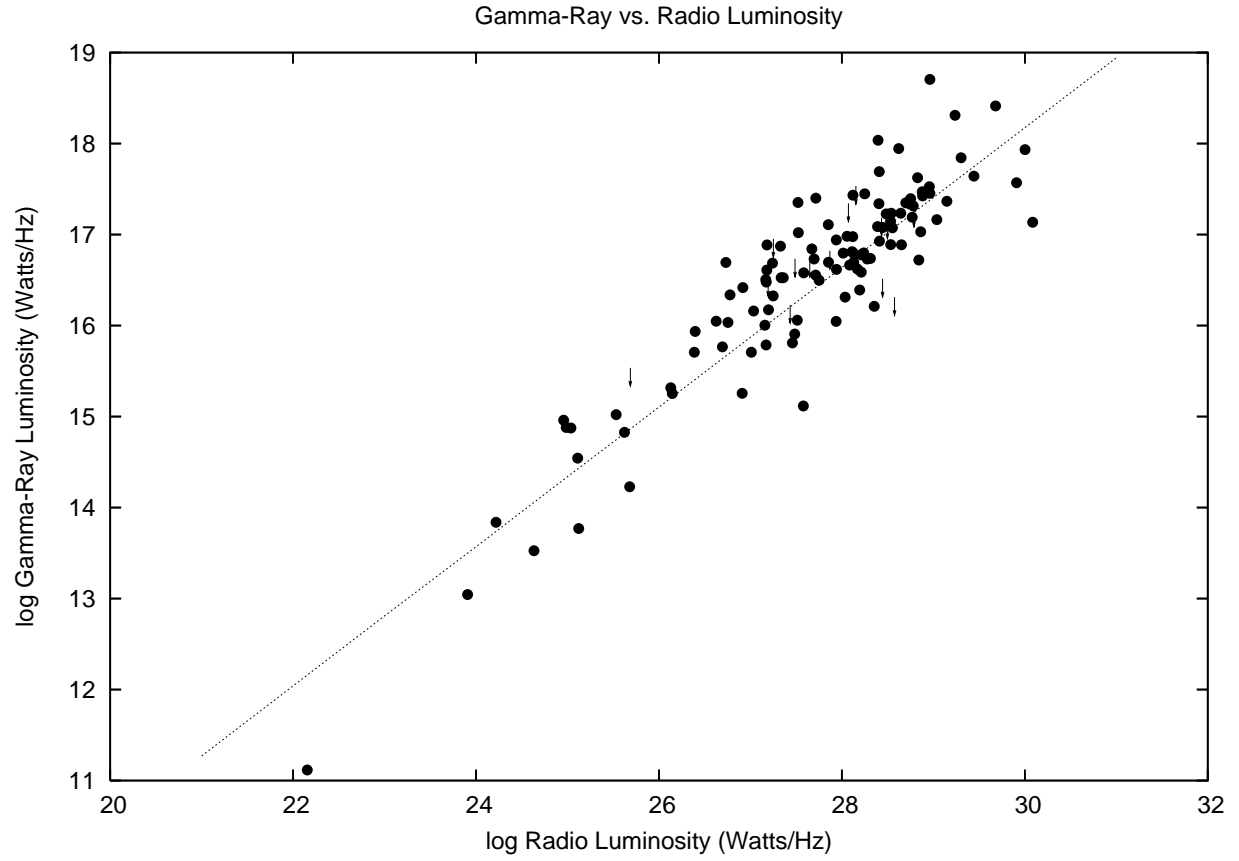


Fig. 1.— The observed radio/gamma ray luminosity correlation. Arrows indicate upper limits and the dashed line represents the regression fit.

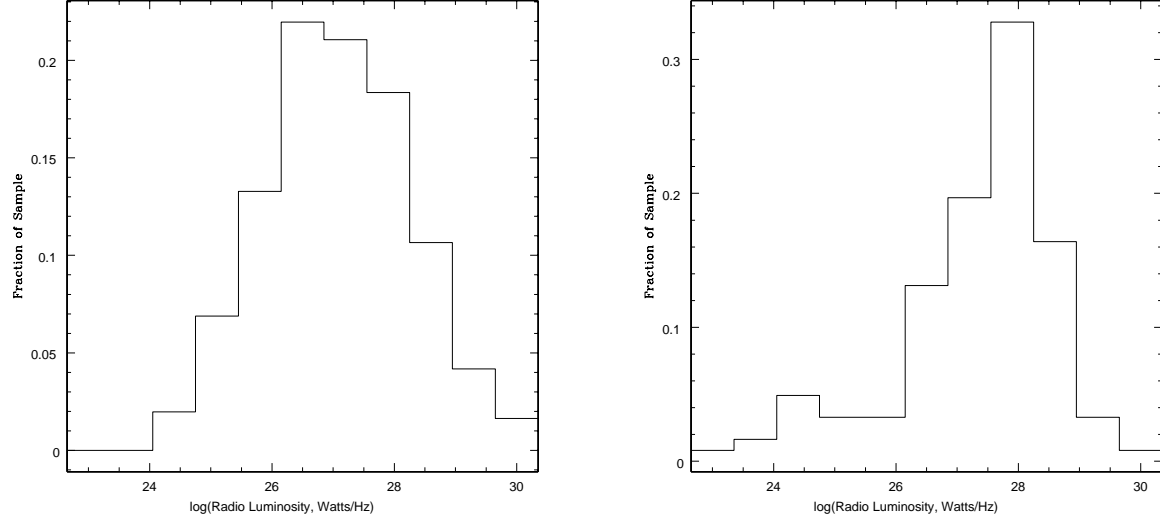


Fig. 2.— Simulated (left) and Observed(right) Radio Luminosity Distributions (SSC model assumed for simulations)

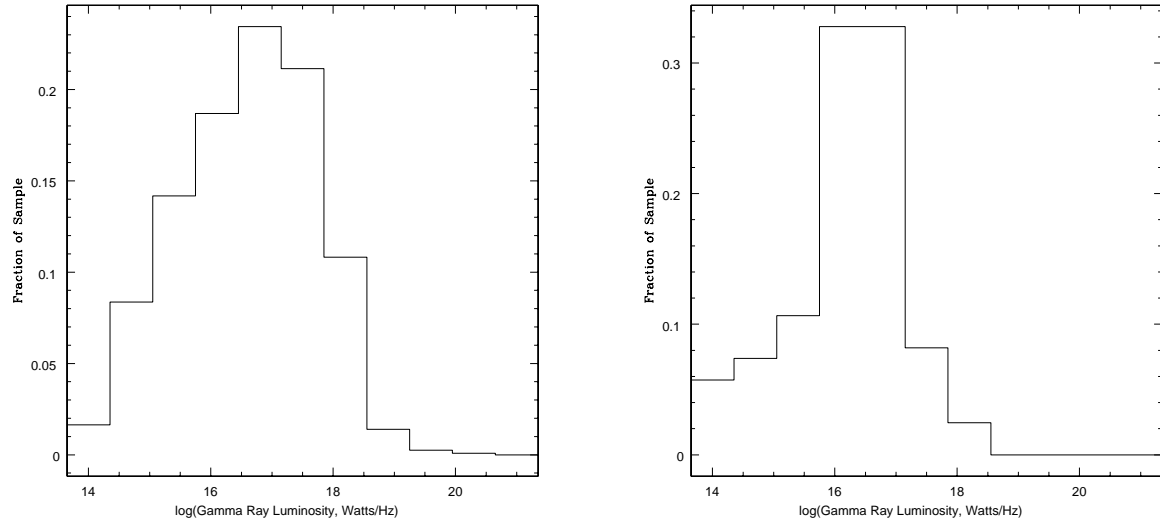


Fig. 3.— Simulated (left) and Observed (right) Gamma Ray Luminosity Distributions (SSC model assumed for simulations)

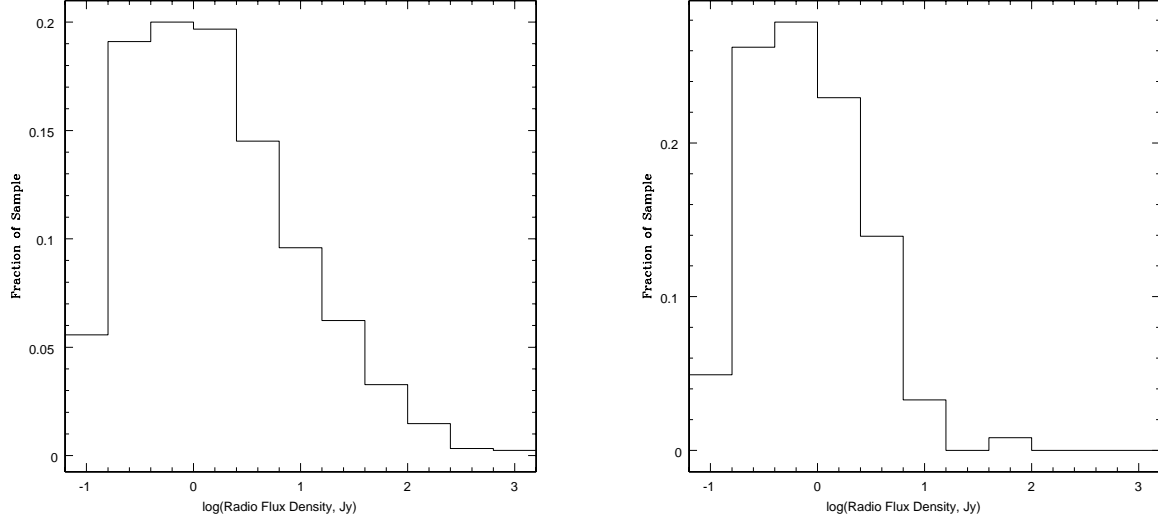


Fig. 4.— Simulated (left) and Observed (right) Radio Flux Density Distributions (SSC model is assumed for simulations)

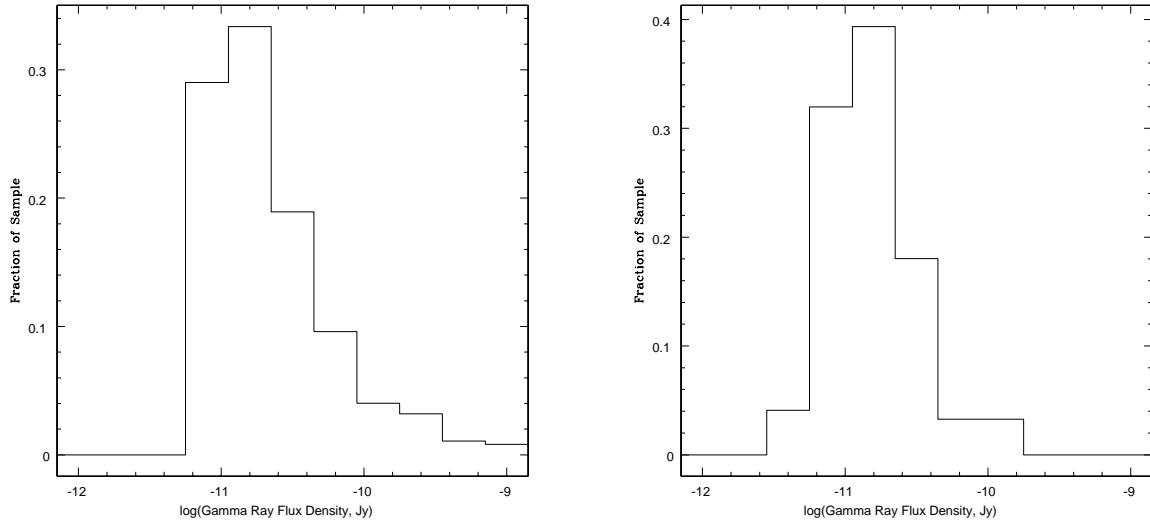


Fig. 5.— Simulated (left) and Observed (right) Gamma Ray Flux Density Distributions (SSC model is assumed for the simulations)

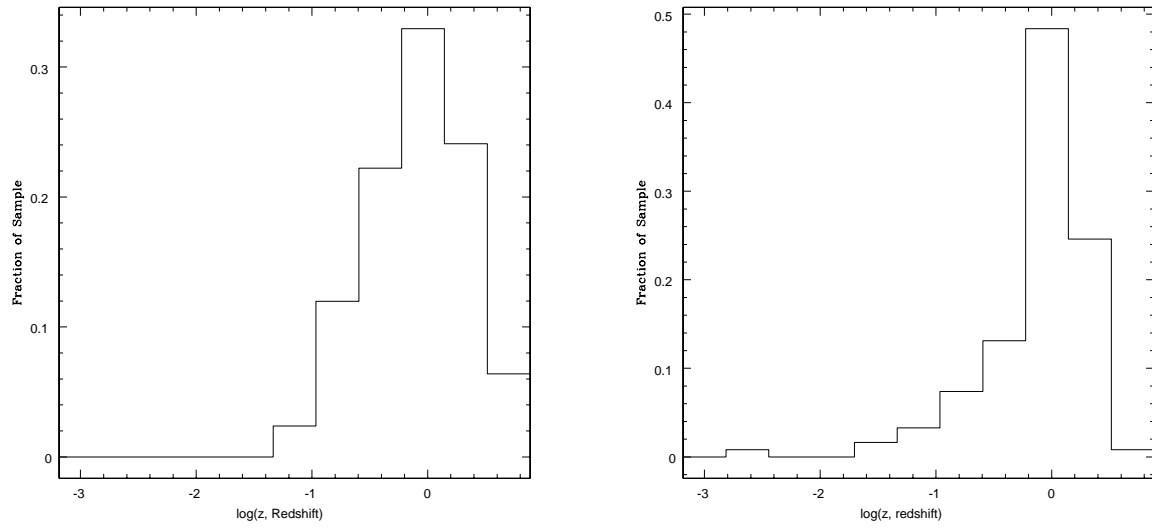


Fig. 6.— Simulated (left) and Observed (right) Redshift Distributions (SSC model is assumed for the simulations)

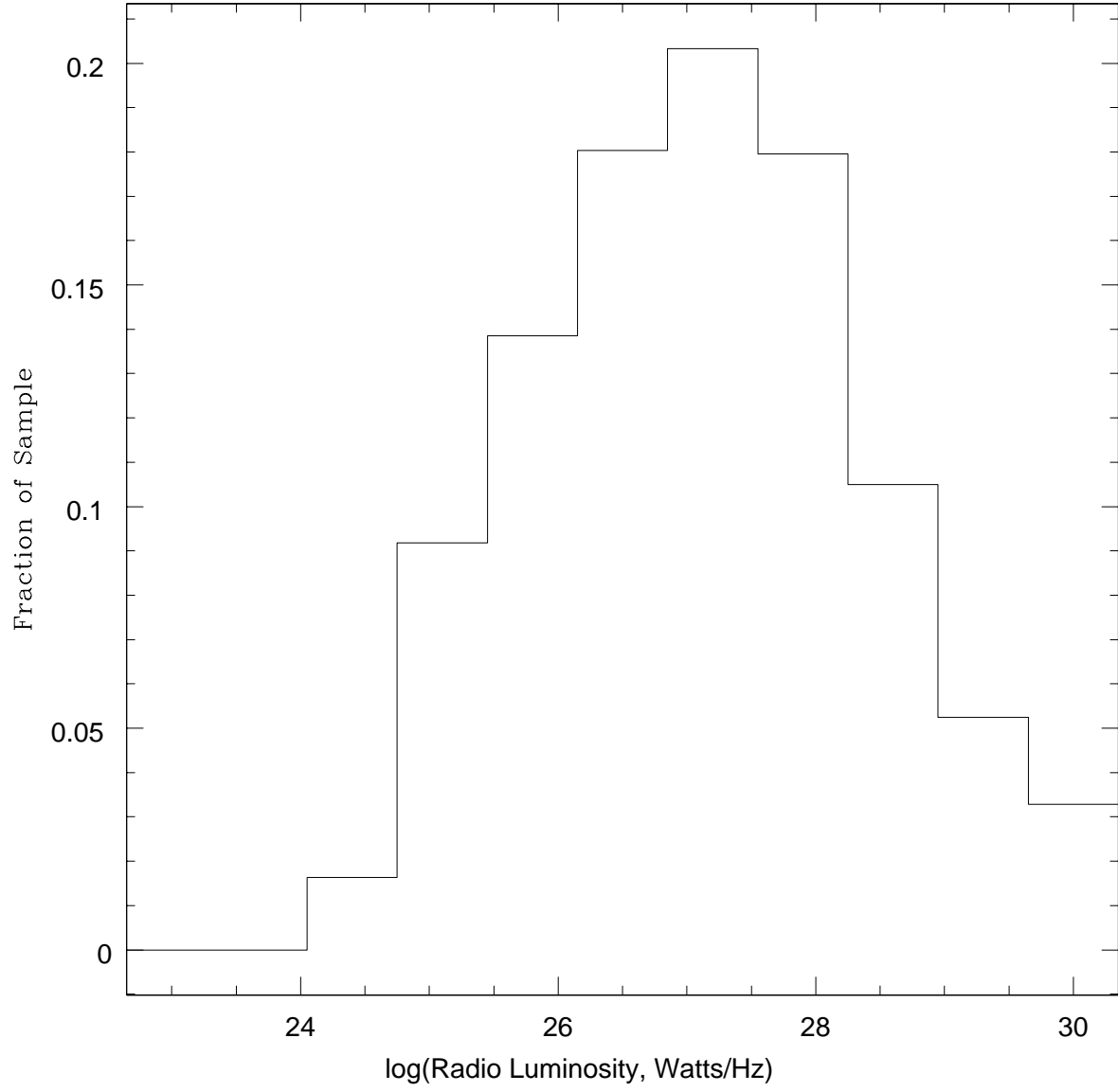


Fig. 7.— Simulated Radio Luminosity Distribution (ECS model is assumed)

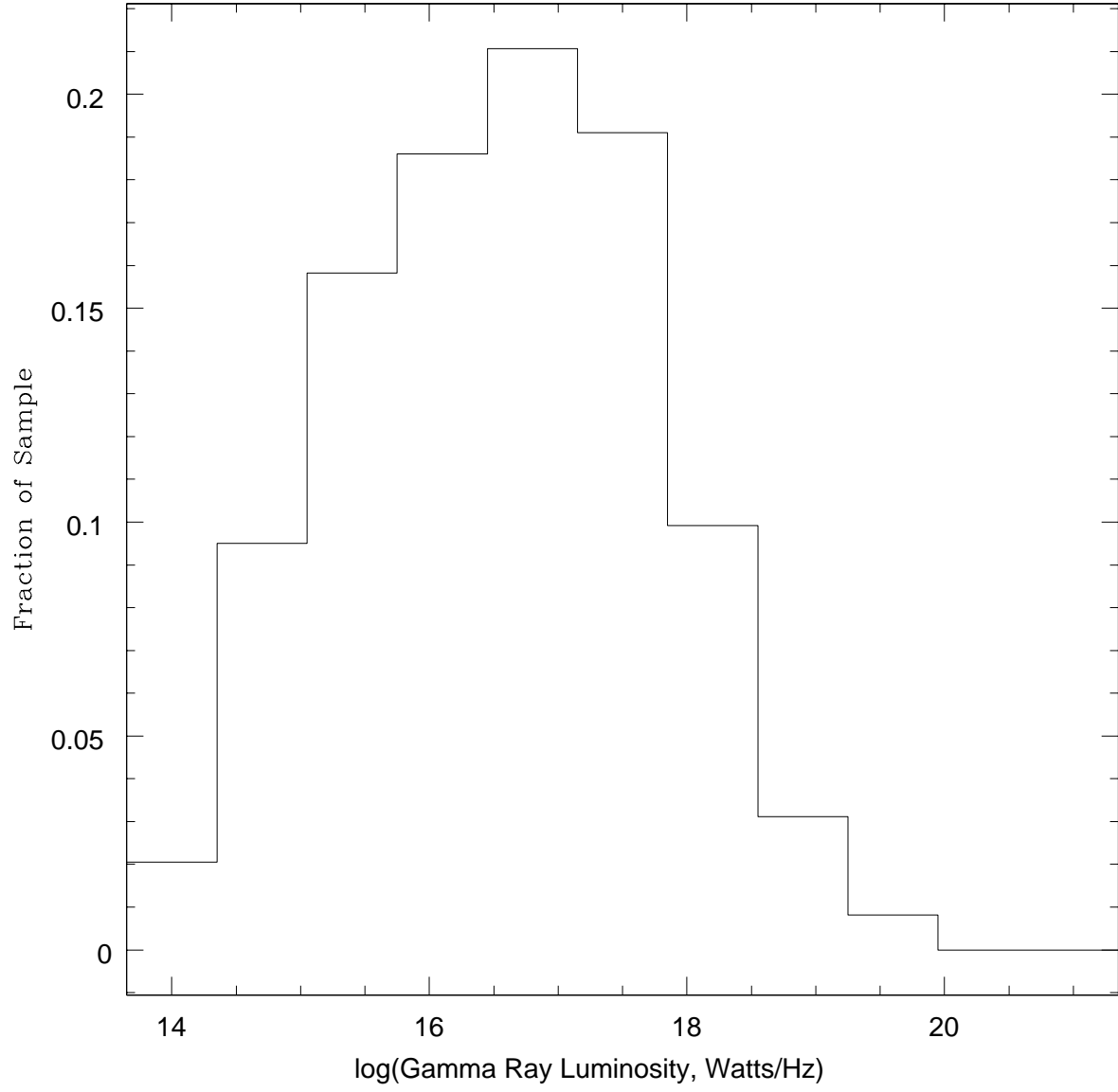


Fig. 8.— Simulated Gamma Ray Luminosity Distribution (ECS model is assumed)

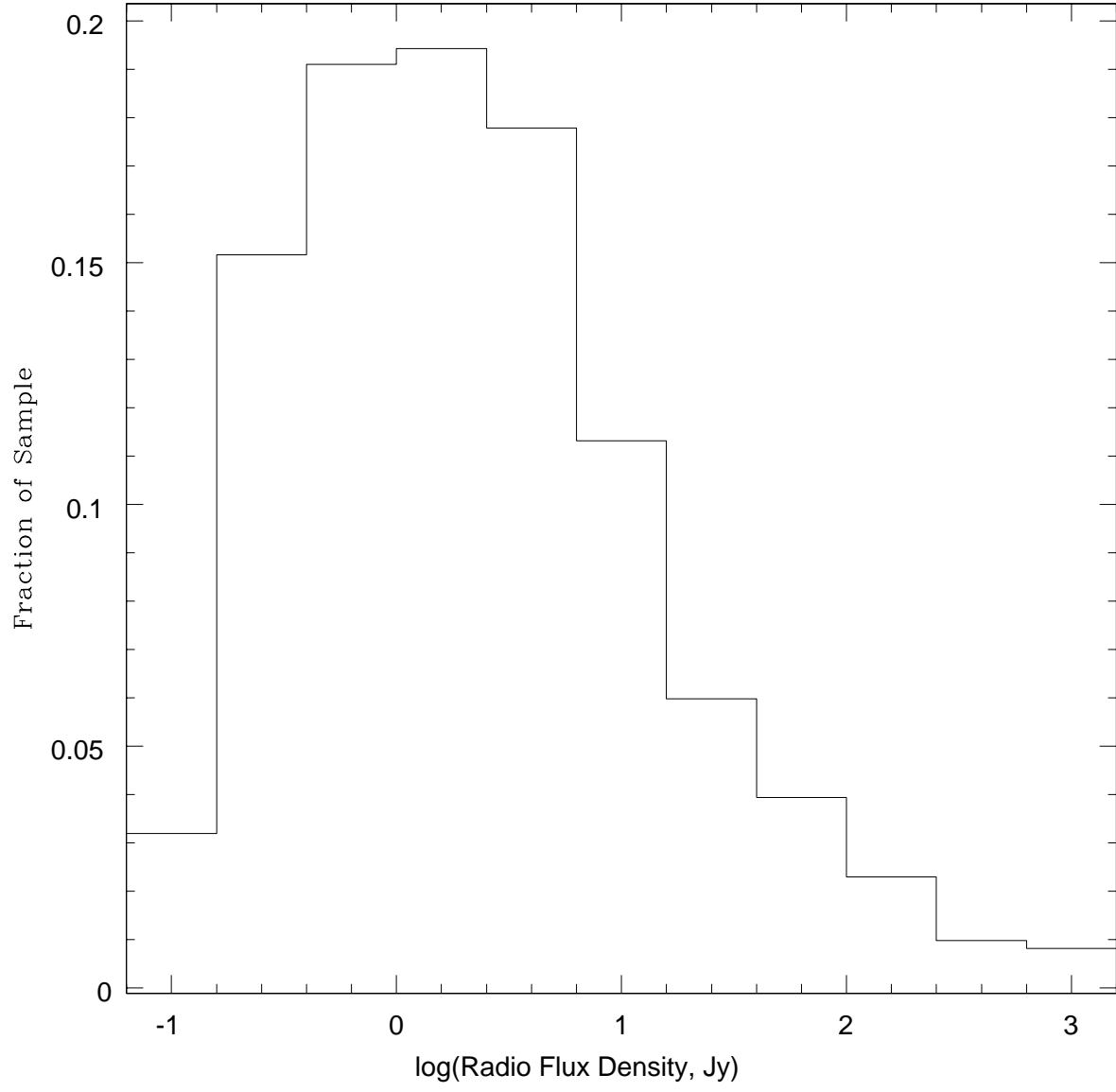


Fig. 9.— Simulated Radio Flux Density Distribution (ECS model is assumed)

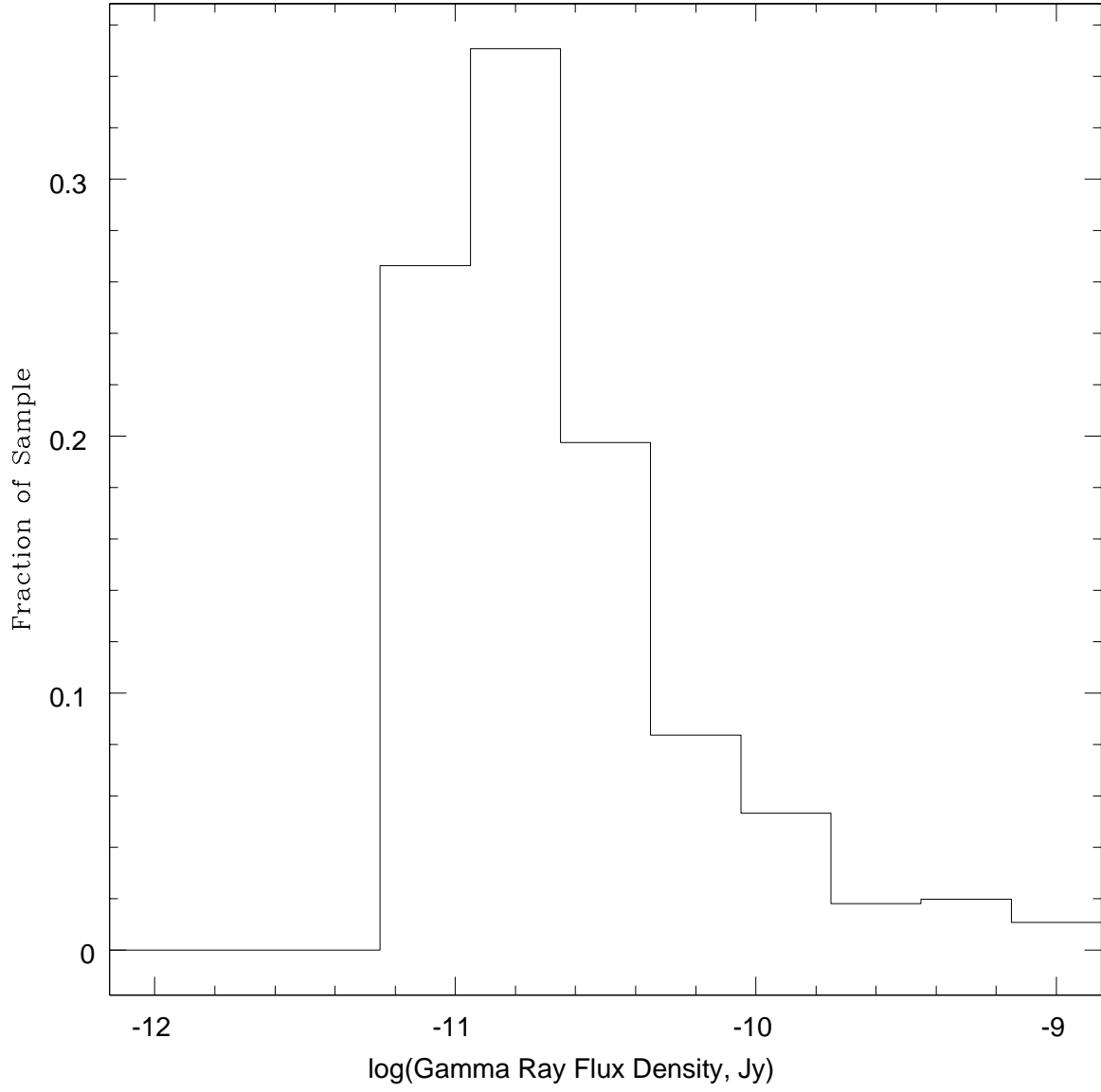


Fig. 10.— Simulated Gamma Ray Flux Density Distribution (ECS model is assumed)

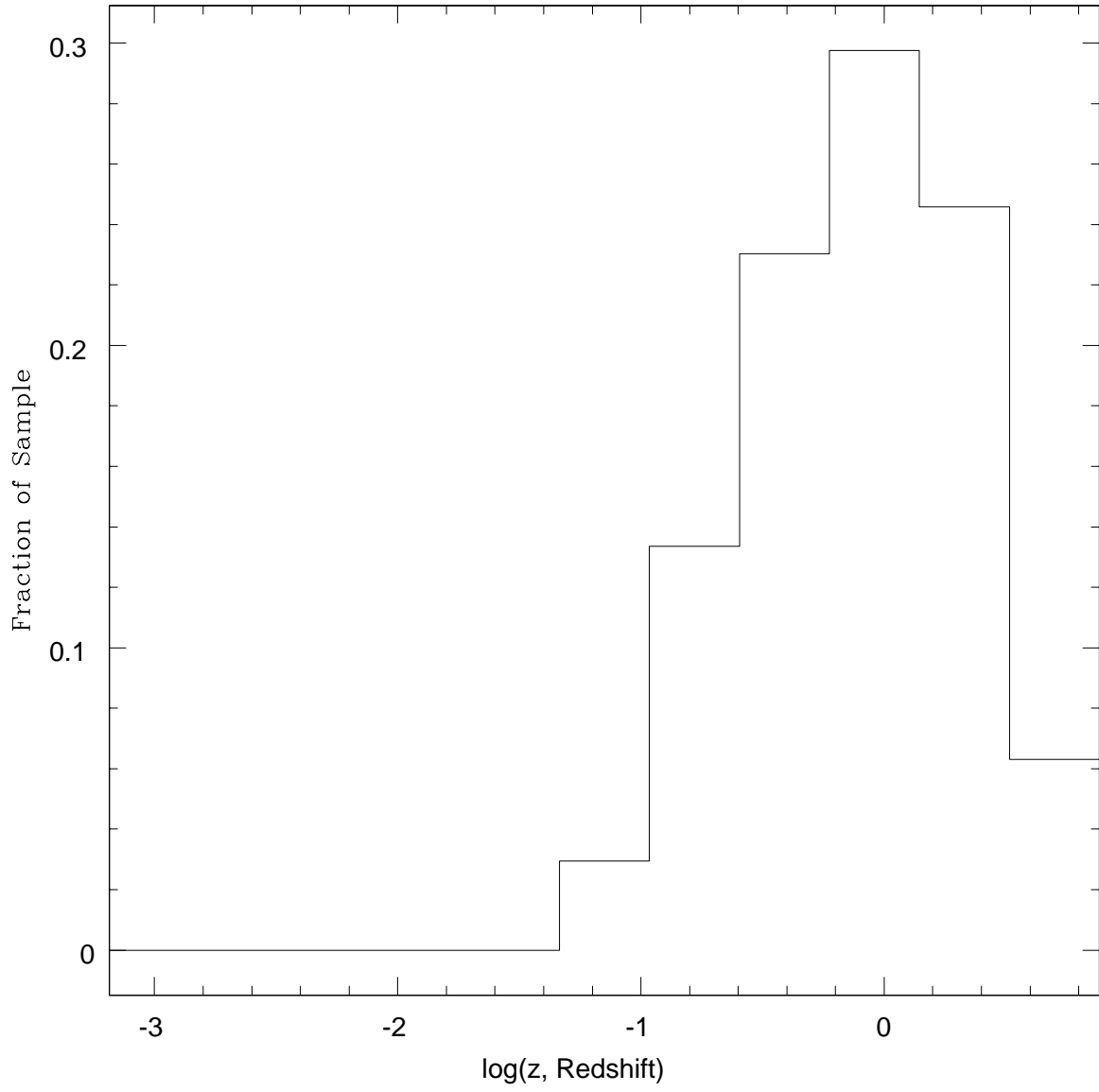


Fig. 11.— Simulated Redshift Distribution (ECS model is assumed)

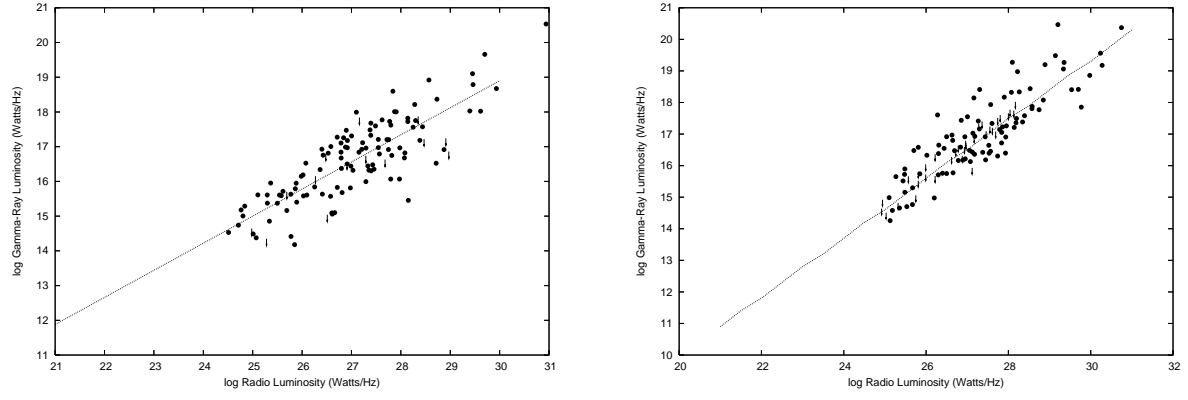


Fig. 12.— Simulated Radio/Gamma-Ray Luminosity Correlation Diagrams for SSC (left) and ECS (right). The arrows indicate upper limits and the dashed line indicates the regression fit.

Table 1. Multiwaveband Data for EGRET Blazars

EGRET Source	Radio Source	z	$\log L_r$ ($Watts\ Hz^{-1}$)	$\log L_o$ ($Watts\ Hz^{-1}$)	$\log L_g$ ($Watts\ Hz^{-1}$)	α_r	α_g	α_{ro}	α_{og}	δ_{var}	Ref
(1)	(2)	(3)	(4)	(5)	(6)	(7)	(8)	(9)	(10)	(11)	(12)
3EG J0038-0949	J0039-0942	2.101	28.030	24.41	16.96	-0.12	1.7	0.69	0.83	0	2,1,6,3
3EG J0118+0248	J0113+0222	0.047	24.26	23.38	13.15	-0.1	1.63	0.18	1.24	1.18	1,1,1,3
3EG J0130-1758	J0132-1654	1.022	27.74	23.80	16.44	-0.08	1.5	0.78	0.86	0	2,2,4,3
3EG J0204+1458	J0204+1514	0.405	27.11	21.29	15.53	0.09	1.23	1.20	0.68	1.29	7,1,5,3
3EG J0210-5055	J0210-5101	0.999	28.25	24.39	17.57	-0.07	0.99	0.78	0.81	0.31	14,15,4,3
3EG J0215+1123	J0213+1213	0.252	25.31	21.57	< 15.16	-0.1	1.03	0.77	0.77	1.27	1,1,1,3
3EG J0222+4253	J0222+4302	0.444	26.54	24.11	16.04	0.17	1.01	0.50	0.97	0	4,1,4,3
3EG J0239+2815	J0237+2848	1.213	28.48	23.83	16.65	-0.1	1.53	0.93	0.83	0	4,1,4,3
3EG J0237+1635	J0238+1636	0.94	28.51	23.48	17.05	-0.5	0.85	0.98	0.77	0.89	4,1,4,3
3EG J0245+1758	J0242+1742	0.551	26.38	22.22	15.66	-0.1	1.61	0.84	0.77	1.14	1,1,1,3
3EG J0329+2149	J0325+2224	2.066	28.39	24.24	16.82	0	1.61	0.81	0.83	0	1,1,1,3
3EG J0340-0201	J0339-0146	0.852	28.02	23.61	16.71	-0.13	0.84	0.88	0.72	0	4,1,4,3
3EG J0404+0700	J0407+0742	1.133	27.75	24.29	16.42	-0.3	1.65	0.67	0.91	0.39	1,1,1,3
3EG J0412-1853	J0416-1851	1.536	28.07	24.27	< 16.14	0.23	2.25	0.77	0.90	0	4,1,4,3
3EG J0422-0102	J0423-0120	0.915	28.28	24.95	16.51	-0.2	1.44	0.65	0.99	0	4,1,4,3
3EG J0423+1707	J0422+1741	0.908	26.95	23.14	16.50	-0.5	1.43	0.73	0.77	0.42	1,1,1,3
3EG J0433+2908	J0433+2905	...	27.34	23.43	17.03	0	0.9	0.78	0.76	0.40	..., 1,3
3EG J0442-0033	J0442-0017	0.844	27.32	23.27	16.36	0.39	1.37	0.84	0.81	1.59	4,1,4,3
3EG J0450+1104	J0449+1121	1.207	28.11	23.44	16.85	-0.2	1.27	1.06	0.69	1.13	5,1,5,3
3EG J0456-2338	J0457-2324	1.003	27.98	23.66	15.84	0	2.14	0.84	0.9	0.21	5,1,5,3
3EG J0458-4635	J0455-4615	0.858	27.66	24.02	15.94	0.18	1.75	0.74	0.94	0.41	4,15,4,3
3EG J0459+0544	J0502+0609	1.106	27.48	23.40	16.32	0.28	1.36	0.82	0.83	0.74	5,1,5,3
3EG J0459+3352	J0503+3403	0.149	25.16	22.02	14.64	0.38	1.54	0.65	0.89	0.59	1,1,1,3
3EG J0500-0159	J0501-0159	2.2286	29.53	24.76	17.20	-0.25	1.45	0.91	0.86	1.09	4,2,4,3
3EG J0510+5545	J0514+5602	2.19	28.02	23.50	17.66	0.18	1.19	0.91	0.67	0	1,1,1,3
3EG J0512-6150	J0506-6109	1.093	27.90	24.52	16.36	0.21	1.40	0.68	0.95	0	4,15,4,1
3EG J0530-3626	J0529-3555	...	27.29	24.08	16.47	-0.42	1.63	0.64	1.04	0.58	..., 2,7,3
3EG J0530+1323	J0530+1331	2.07	29.31	24.03	18.04	-0.3	1.46	1.01	0.55	0.74	5,1,5,3
3EG J0531-2940	J0539-2839	3.104	29.07	24.52	17.27	0.06	1.47	0.89	0.81	0.85	4,2,4,3
3EG J0533+4751	J0533+4822	1.16	27.68	23.67	16.61	-0.1	1.55	0.75	0.84	0.0	1,1,1,3
3EG J0540-4402	J0538-4405	0.896	28.56	25.20	17.08	-0.17	1.41	0.66	0.95	0.75	4,15,4,3
3EG J0542-0655	J0541-0541	0.839	27.49	22.95	< 16.45	-0.06	1.0	0.91	0.77	1.38	5,2,5,3
3EG J0542+2610	J0540+2507	0.62	26.40	24.56	15.96	0.12	1.67	0.90	0.70	0.57	1,1,1,3
3EG J0721+7120	J0721+1721	0.3	26.02	23.61	15.56	0.09	1.19	0.49	0.97	0	4,1,4,3
3EG J0737+1721	J0738+1742	0.424	27.14	24.24	15.69	-0.1	1.6	0.58	1.02	0	4,1,4,3
3EG J0743+5447	J0742+5444	0.723	26.36	24.84	16.32	0.36	1.03	0.55	0.88	1.21	5,1,5,3
3EG J0808+5114	J0807+5117	1.14	27.57	23.95	16.24	-0.4	1.76	0.69	0.88	0	5,1,5,3
3EG J0828+0508	J0831+0429	0.1736	25.77	22.65	14.88	0	1.47	0.64	0.93	0	4,1,4,3
3EG J0829+2413	J0830+2410	0.939	27.48	24.18	16.73	0	1.42	0.66	0.87	...	4,1,4,3
3EG J0845+7049	J0841+7053	2.172	28.77	25.49	16.99	0.42	1.62	0.67	0.96	0.62	4,1,4,3
3EG J0852-1216	J0850-1213	0.566	26.87	23.77	16.31	-0.37	0.58	0.61	0.90	1.21	5,2,5,3
3EG J0853+1941	J0854+2006	0.306	26.80	24.23	15.41	-0.3	1.03	0.51	1.06	0	4,1,4,3
3EG J0917+4427	J0920+4441	2.18	28.93	24.49	17.47	-0.1	1.19	0.86	0.81	0.0	4,1,4,3
3EG J0952+5501	J0957+5522	0.901	27.64	23.87	16.42	0.39	1.12	0.78	0.88	0.39	4,1,4,3
3EG J0958+6533	J0958+6533	0.368	26.64	24.70	15.33	-0.3	1.08	0.38	0.88	0.96	4,1,4,3
3EG J1052+5718	J1058+5628	0.14	25.88	23.54	15.18	0.09	1.51	0.31	1.09	0.24	5,1,5,3
3EG J1104+3809	J1104+3812	0.031	23.85	22.32	13.46	0	0.57	0.32	1.07	0.35	4,1,4,3
3EG J1133+0033	J1133+0040	1.633	27.84	24.07	16.21	0.05	1.73	0.74	0.89	0.82	1,1,1,3
3EG J1200+2847	J1159+2914	0.729	27.34	23.99	16.18	0.24	0.98	0.68	0.93	1.17	4,1,4,3
3EG J1219-1520	J1222-1645	...	26.87	23.42	15.95	0.03	1.52	0.65	0.89	1.10	..., 2,8,3
3EG J1222+2841	J221+2813	0.102	25.25	22.13	14.45	-0.2	0.73	0.64	0.93	0.62	4,1,4,3
3EG J1224+2118	J1224+2122	0.435	26.66	23.20	15.79	0.34	1.28	0.71	0.88	0.45	4,1,4,3
3EG J1227+4302	J1224+4335	1.872	27.69	23.74	< 16.97	0.26	1.5	0.80	0.79	1.36	1,1,1,3
3EG J1229+0210	J1229+0203	0.158	27.20	24.02	14.74	0.04	1.58	0.65	1.12	0.46	4,1,4,3
3EG J1236+0457	J1231+0418	1.03	27.21	23.99	16.21	0.05	1.48	0.64	0.91	0.53	1,1,1,3
3EG J1246-0651	J1246-0730	1.286	27.86	24.26	16.42	-0.08	1.73	0.71	0.6	...	4,2,4,3
3EG J1255-0549	J1256-0547	0.538	28.16	23.34	16.86	-0.2	0.96	0.97	0.78	0.9	4,2,4,3
3EG J1310-0517	J1312-04242	0.824	26.96	23.24	16.15	-0.15	1.34	0.76	0.82	...	1,1,1,3
3EG J1323+2200	J1327+2210	1.40	28.66	24.06	16.79	-0.5	0.86	0.74	0.95	1.09	5,1,5,3
3EG J1324-4314	J1325-4301	0.0018	21.78	22.00	10.74	0.66	1.58	-0.05	1.36	0	16,7,13,3
3EG J1329+1708	J1333+1649	2.09	29.71	25.36	16.76	-0.1	1.41	0.57	0.99	0.62	4,1,4,3
3EG J1339-1419	J1337-1257	0.539	27.56	23.56	15.67	-0.21	1.62	0.80	0.93	0.81	4,2,4,3
3EG J1347+2932	J1343+2844	0.91	26.81	24.24	16.24	0.13	1.51	0.51	0.93	0.64	9,1,9,3
3EG J1409-0745	J1408-0752	1.494	28.03	24.28	17.32	0	1.29	0.74	0.81	1.42	4,2,4,3

Table 1—Continued

EGRET Source	Radio Source	z	$\log L_r$ (Watts Hz ⁻¹)	$\log L_o$ (Watts Hz ⁻¹)	$\log L_g$ (Watts Hz ⁻¹)	α_r	α_g	α_{ro}	α_{og}	δ_{var}	Ref
(1)	(2)	(3)	(4)	(5)	(6)	(7)	(8)	(9)	(10)	(11)	(12)
3EG J1424+3734	J1419+3821	1.83	28.47	24.08	16.35	-0.1	2.25	0.85	0.84	...	4,1,4,3
3EG J1429-4217	J1427-4206	1.522	28.59	24.16	17.08	0.15	1.13	0.80	0.88	0.93	4,1,4,3
3EG J1457-1903	J1459-1810	...	26.98	<24.60	16.15	-0.24	1.67	0.78	0.79	0.49	..., 2,7,3
3EG J1500-3509	J1457-3539	1.422	27.94	23.97	16.36	0.04	1.99	0.79	0.85	0	2,2,2,3
3EG J1504-1537	J1502-1508	...	26.88	<23.02	<16.58	-0.18	...	0.76	0.76	1.24	..., 2, ..., 3
3EG J1512-0849	J1512-0905	0.360	26.78	23.39	15.63	0.12	1.47	0.69	0.92	0	4,2,4,3
3EG J1517-2538	J1517-2422	0.049	24.75	19.84	13.39	0.02	1.66	1.02	0.75	0	2,2,2,3
3EG J1527-2358	J1532-2310	2.289	28.06	24.11	<16.81	-0.09	1.67	0.76	0.81	0.92	2,2,2,3
3EG J1605+1553	J1603+1554	0.11	24.66	23.77	14.50	-0.5	1.47	0.17	1.12	0	1,1,1,3
3EG J1608+1055	1608+1029	1.23	28.27	23.59	16.86	-0.1	1.06	0.84	0.82	1.09	5,1,5,3
3EG J1607-1101	J1612-1133	...	27.11	<23.02	<16.36	-0.58	...	0.78	0.79	1.45	..., 2, ..., 3
3EG J1612-2618	J1611-2612	...	26.80	<23.02	16.10	-0.17	1.71	0.75	0.79	1.04	..., 2, ..., 3
3EG J1614+3424	J1613+3412	1.40	28.58	24.56	17.15	0.13	1.42	0.81	0.86	0	4,1,4,3
3EG J1621+8203	J1632+8232	0.02	23.53	21.93	12.67	0.05	1.29	0.33	1.11	0	5,2,7,3
3EG J1625-2955	J1626-2951	0.815	27.75	23.18	17.06	0.00	1.07	1.02	0.67	1.62	5,2,5,3
3EG J1626-2519	1625-2527	0.786	27.74	22.63	16.60	0.45	1.21	1.17	0.65	1.05	5,2,5,3
3EG J1634-1434	J1628-1415	1.025	27.15	23.08	16.65	0.14	1.15	0.82	0.76	0	4,2,4,3
3EG J1635-1751	J1629-1720	...	27.27	<22.96	<16.36	-0.56	...	0.83	0.78	0.83	..., 2, ..., 3
3EG J1635+3813	J1635+3808	1.81	28.86	24.79	17.94	0.04	1.15	0.80	0.79	0	4,1,4,3
3EG J1646-0704	J1644-0743	0.139	24.58	20.44	14.59	-0.08	1.39	0.85	0.70	0.75	2,2,2,3
3EG J1718-3313	J1717-3342	...	27.56	<22.96	16.57	-0.06	1.59	0.92	0.74	0.82	..., 2, ..., 3
3EG J1720-7820	1723-7713	...	27.38	23.61	16.12	-0.55	1.74	0.69	0.88	0.64	..., 7,8,3
3EG J1727+0429	J1728+0427	0.29	26.01	22.97	15.33	0.04	1.67	0.62	0.91	0	4,1,4,3
3EG J1733+6017	J1722+6105	2.06	28.04	24.07	16.55	-0.1	2.0	0.75	0.83	0.29	1,1,1,3
3EG J1733-1313	1733-1304	0.9	28.37	23.63	16.96	-0.02	1.23	0.95	0.78	0.37	4,2,4,3
3EG J1735-1500	J1738-1503	...	27.43	23.33	<16.23	0.15	2.24	0.83	0.80	0.87	10,2,10,3
3EG J1738+5203	J1740+5211	1.38	28.33	24.14	16.97	-0.2	1.42	0.81	0.83	0.51	4,1,4,3
3EG J1744-0310	J1743-0350	1.05	28.16	23.78	16.52	-0.22	1.42	0.86	0.84	0.59	4,1,4,3
3EG J1800-3955	J1802-3940	...	26.79	22.80	15.27	0.07	2.1	0.82	0.91	0	17,2, ..., 3
3EG J1806-5005	J1808-5011	1.61	27.80	23.63	16.25	-0.33	1.93	0.84	0.82	0.88	12,7,12,3
3EG J1824+3440	J1826+3431	1.81	27.78	25.23	<17.16	0.25	1.03	0.51	0.95	0.01	1,1,1,3
3EG J1828+0142	J1826+0149	1.77	28.41	25.98	<16.91	-0.2	1.76	1.01	0.70	1.6	1,1,1,3
3EG J1832-2110	J1833-2103	2.510	29.63	23.46	17.56	0.25	1.59	1.25	0.64	0.62	5,2,5,3
3EG J1850-2652	J1848-2718	...	27.71	<22.96	16.29	-1.26	1.19	0.88	0.78	0.81	..., 2, ..., 3
3EG J1904-1124	J1905-1153	...	26.81	<22.96	16.51	0.26	1.6	0.79	0.75	0.08	..., 2, ..., 3
3EG J1911-2000	J1911-2006	1.119	28.16	23.73	16.77	0.11	1.39	0.89	0.81	0.3	11,2,11,3
3EG J1921-2015	J1923-2104	0.871	27.82	24.11	<16.15	0.19	0.75	0.95	1.24	...	11,2,11,3
3EG J1935-4022	J1937-3958	0.965	27.82	23.58	16.02	-0.15	1.86	0.77	0.91	1.34	5,2,5,3
3EG J1937-1529	J1939-1525	1.66	28.20	24.76	<15.94	0.0	2.45	0.83	0.88	1.35	4,2,4,3
3EG J1959+6342	J2006+6424	1.57	28.41	<23.50	16.94	-0.3	1.45	0.95	0.75	0	5,1,5,3
3EG J2006-2321	J2005-2310	0.830	26.79	23.29	16.13	0.14	1.33	0.71	0.84	1.31	2,2,2,3
3EG J2025-0744	J2025-0735	1.388	27.88	24.15	17.07	0.33	1.38	0.76	0.82	0.87	5,2,5,3
3EG J2027+3429	J2025+3343	0.22	26.32	21.08	15.39	-0.4	1.28	1.07	0.68	0	1,1,1,3
3EG J2034-3110	J2030-3039	...	27.08	25.10	15.44	-0.05	2.43	0.82	0.84	1.18	12,2,12,3
3EG J2036+1132	J2034+1154	0.60	26.82	23.13	15.80	0.46	1.83	0.73	0.85	0	5,1,5,3
3EG J2046+0933	J2049+1003	...	27.84	<22.96	16.40	-0.6	1.22	0.94	0.77	0	..., ..., 1,3
3EG J2055-4716	J2056-4714	1.49	28.38	23.99	17.02	0.32	1.04	0.89	0.82	0.93	4,15,4,3
3EG J2100+6012	J2102+6015	4.57	28.59	26.13	18.33	0.35	1.21	0.52	0.88	0.13	2,2,2,3
3EG J2158-3023	J2158-3013	0.12	24.61	23.29	14.51	0.44	1.35	0.27	1.06	0.59	4,2,4,3
3EG J2202+4217	J2202+4216	0.07	25.31	22.58	13.85	0.31	1.6	0.57	1.05	0.8	1,1,4,3
3EG J2206+6602	J2208+6519	1.12	27.14	22.69	16.98	0.33	1.29	0.91	0.66	0	1,1,1,3
3EG J2209+2401	J2212+2355	1.13	27.76	23.70	16.32	-0.1	1.48	0.80	0.86	0.91	1,1,1,3
3EG J2232+1147	J2232+1143	1.04	28.08	24.27	16.70	0.48	1.45	0.79	0.88	0.48	4,1,4,3
3EG J2254+1601	J2253+1608	0.86	28.50	24.54	17.10	0.1	1.21	0.80	0.88	0.52	4,1,4,3
3EG J2255+1943	J2253+1942	0.28	25.75	22.53	14.94	-0.1	1.36	0.66	0.91	1.18	5,1,4,3
3EG J2321-0328	J2323-0317	1.411	28.12	24.13	<16.78	0.0	...	0.79	0.87	1.36	4,2,4,3
3EG J2358+4604	J2354+4553	1.99	28.45	23.74	17.25	0.34	1.38	0.96	0.74	0	4,1,4,3
3EG J2359+2041	J0003+2129	0.45	26.25	21.58	15.67	-0.6	1.09	0.93	0.71	0.74	1,1,1,3

References. — (1) Sowards-Emmerd *et al.* 2003 (2) Sowards-Emmerd *et al.* 2004 (3) Hartman *et al.* 1999 (4) Hewitt & Burbidge 1989 (5) Veron-Cetty & Veron 2001 (6) Bloom *et al.* 2004 (7) NED (8) Monet *et al.* (9) Stocke *et al.* 1991 (10) Combi *et al.* (11) Halpern *et al.* 2003 (12) Landt *et al.* 2001 (13) Lauberts & Valentijn 1989 (14) Wisotzki *et al.* 2000 (15) Wright & Otrupcek 1990 (16) Fouque *et al.* (17) Liang & Liu 2003

Table 2. Correlation and Regression Analysis for EGRET Blazars

Ind. Var. (1)	Dep. Var. (2)	N (3)	τ (4)	Prob. (5)	ρ (6)	Prob. (7)	Technique (8)	Slope (9)	Intercept (10)
$\log L_r$	$\log L_\gamma$	122	0.628	1×10^{-10}	0.806	1×10^{-10}	EM	0.766	-4.81
$\log z$	$\log L_r$	122	0.650	1×10^{-10}	0.825	1×10^{-10}	EM	2.47	27.7
$\log z$	$\log L_\gamma$	122	0.569	1×10^{-10}	0.705	1×10^{-10}	EM	2.12	16.4
$\log L_o$	$\log L_\gamma$	122	0.299	1×10^{-6}	0.437	2×10^{-6}	SB	0.566	2.71
$\log z$	$\log L_o$	122	0.404	1×10^{-10}	0.564	7×10^{-10}	EM	1.26	23.7
α_{ro}	$\alpha_{o\gamma}$	122	-0.556	1×10^{-10}	-0.701	1×10^{-10}	BJ	-0.519	1.23
$\log L_o$	α_{ro}	122	-0.094	0.122	-0.111	0.222	SB	-0.007	0.892
$\log L_o$	$\alpha_{o\gamma}$	122	0.214	7×10^{-4}	0.309	$7. \times 10^{-4}$	SB	0.032	0.113

Table 3. Partial Correlation Analysis for EGRET Blazars

Ind. Var. (1)	Dep. Var. (2)	Third Var. (3)	N (4)	τ (5)	Prob. (6)
$\log L_r$	$\log L_\gamma$	$\log z$	122	0.341	1×10^{-10}
$\log L_o$	$\log L_\gamma$	$\log z$	122	-0.089	0.148
α_{ro}	$\alpha_{o\gamma}$	$\log L_o$	122	0.550	2×10^{-8}

Table 4. Parameters for Monte Carlo Simulations

Identifier (1)	$\log L_1$ (2)	$\log L_2$ (3)	g (4)	Γ_1 (5)	Γ_2 (6)	s (7)	τ (8)	z_{min} (9)	z_{max} (10)	h (11)	K_{min} (12)	K_{max} (13)	slope (14)
Lister SSC	22.4	26.0	2.5	1.001	25.0	1.5	0.26	0.0	4.0	0.65	5×10^{-14}	1.0×10^{-11}	1.6
Lister ECS	22.4	26.0	2.5	1.001	25.0	1.5	0.26	0.0	4.0	0.65	1.0×10^{-16}	1.0×10^{-15}	2.3
Bloom SSC	21.5	30.0	2.0	1.001	30.0	1.5	0.26	0.0	5.0	1.0	5×10^{-14}	1×10^{-11}	1.6
Bloom ECS	21.3	30.0	2.0	1.001	30.0	1.5	0.26	0.0	5.0	1.0	4.8×10^{-17}	5×10^{-17}	2.3

Table 5. Kolmogorov-Smirnov Tests for Monte Carlo Simulations

Identifier (1)	D_{Lr} (2)	Prob (3)	$D_{L,\gamma}$ (4)	Prob (5)	D_z (6)	Prob (7)	D_{fr} (8)	Prob (9)	$D_{f\gamma}$ (10)	Prob (11)
Lister SSC	0.516	1×10^{-15}	0.172	0.054	0.328	4×10^{-6}	0.303	3×10^{-5}	0.148	0.140
Lister ECS	0.426	5×10^{-10}	0.148	0.398	0.271	0.004	0.156	0.103	0.189	0.026
Bloom SSC	0.205	0.012	0.230	0.003	0.180	0.038	0.205	0.012	0.164	0.075
Bloom ECS	0.164	0.075	0.246	0.001	0.213	0.008	0.271	0.003	0.197	0.018